THE JOURNAL OF PHYSICAL CHEMISTRY C
A JOURNAL OF THE AMERICAN CHEMICAL SOCIETY

pubs.acs.org/JPCC

Article

CO_2 Adsorption on Stoichiometric Ceria (110) Revisited

Rolando Saniz,* Shangkun Li, Dirk Lamoen, Annemie Bogaerts, and Bart Partoens*

Cite This: J. Phys. Chem. C 2025, 129, 12814−12826

Read Online

ACCESS | Metrics & More | Article Recommendations | Supporting Information

ABSTRACT: We present a study based on first-principles methods on the adsorption of carbon dioxide on stoichiometric ceria (110) surfaces. We consider all inequivalent potential adsorption sites and different molecule orientations. We find that there are in all five stable adsorption states. The CO_2 molecule either chemisorbs on a surface oxygen or converges to one of four possible physisorption states, depending on the site approached and on the initial molecule orientation. In the chemisorption state, the molecule and surface oxygen form a carbonate species. The binding to the surface is monodentate and strongly involves the CO_2 molecule nonbonding orbitals. Physisorption is of the Debye type, i.e., the interaction occurs due to the induction of a dipole moment on the molecule and the polarization of the on-site surface atoms. In one of the physisorption states, the dipole moment is linear, and physisorption is of moderate strength. In the other three physisorption states, the dipole moment is mainly caused by molecule bending, resulting in stronger physisorption. Our findings suggest that chemisorption should be observed more often than physisorption in this system.

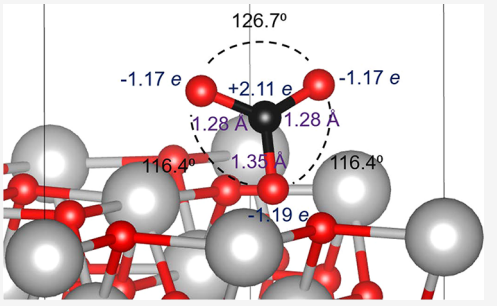

1. INTRODUCTION

Furthering our understanding of the surface chemistry of CO_2 has been at the center of continued research efforts for decades now.[1,2] Environmental problems directly related to CO_2 emissions and the refinement or development of research techniques have fueled even wider and more concerted efforts. For instance, the International Conference on Carbon Dioxide Utilization (ICCDU), a long-running international series, is a forum where topics ranging from fundamental research to industrial applications are discussed every year. Prominent among the topics covered in recent years are catalytic CO_2 splitting, hydrogenation, and conversion. Major technologies for that purpose include thermal, photochemical, electrochemical, and plasma catalysis. The latter has emerged as a prime technology because of the various technical and practical advantages it presents.[3−5] It has been applied in CO_2 hydrogenation research as it is one of the especially promising applications of plasma catalysis.[6,7]

Needless to say, the choice of catalyst is as critical for traditional heterogeneous catalysis as for all of the above technologies. Thus, over the years, a wide range of materials have been used or considered as possible catalysts, depending on the application envisaged.[1,2,8] Experimentally, there has long been interest in transition metal oxides, with works frequently addressing specifically CO_2 adsorption on a range of such oxides, some investigating in particular whether chemisorption and/or physisorption occurs.[1,9−12] From a theoretical point of view, studies based on density functional theory have benefited from the more recent development of reliable approximation methods and functionals to treat the van der Waals interaction. Indeed, it is important to recognize that the van der Waals interaction can significantly affect the adsorption process and the adsorption energies.[13] There are quite remarkable works studying specifically the interplay between physisorption and chemisorption, and showing how the former can lead to the latter.[14−17] As could be expected, most current works concerning CO_2 adsorption exploit those approximation methods and functionals.[18−20]

Ceria and ceria-based materials have long been used as catalysts with success, with the automotive three-way catalysis arguably being its most successful early technological application.[21,22] Interest in ceria as a catalyst on a wider range of applications has thereafter grown steadily, especially in the past decade.[23−26] Not surprisingly, ceria has been considered by many experimental and theoretical groups as a possible catalytic material for the purposes of CO_2 hydrogenation or reduction,[27−32] and, more generally, conversion.[33−37] These works contribute greatly to the development of strategies to convert CO_2 to high-value products. However, as the focus of these works is mainly on the development of the particular catalytic processes considered, there are fundamental aspects of CO_2 adsorption on ceria that have not been addressed directly. In particular, the phenomena determining the adsorption on stoichiometric CeO_2 (110) surfaces, adsorption typically considered in the mentioned works.

Received: March 15, 2025
Revised: May 30, 2025
Accepted: June 26, 2025
Published: July 2, 2025

Note that, because of its structure, and unlike the water molecule, the dipole moment of the CO_2 molecule is zero and only presents a quadrupole moment.[38] Molecular quadrupole moments, however, are in general not expected to lead to a significant molecule−surface interaction if the molecule is not close to its equilibrium position.[39−41] Moreover, in this context, it is important to recall that the CeO_2 (110) free surface is nominally nonpolar. Thus, whether physisorbed or chemisorbed, a quite intriguing question is what mechanism and what changes in the molecular and surface structure and energy levels lead to one or the other adsorption.

It also calls our attention that the different computational works in the reports above, all based on density functional theory (DFT), are not always consistent with each other and show puzzling quantitative and even qualitative differences. Indeed, the earlier studies suggested that CO_2 would only physisorb and not chemisorb on stoichiometric ceria (110) surfaces.[27,28] The more recent works, however, all indicate that CO_2 can chemisorb on such surfaces, at an oxygen site.[34−37] On the other hand, while refs 34 and 35 mention only chemisorption and ref 37 indicates that no stable physisorption was found, ref 36 reports both physisorption and chemisorption. Furthermore, the chemisorption energies at a surface oxygen reported are all different and vary from −1.32 eV in ref 34 to −0.32 eV in ref 36. Also, in refs 36 and 37, the CO_2 molecule chemisorbed at the surface oxygen appears to be rotated by approximately 90° compared to what is found in refs 34 and 35. It is also surprising that while in refs 34 and 35 the molecule will chemisorb preferentially at an oxygen vacancy, i.e., the adsorption energy in that case is lower than in the case of adsorption at a surface oxygen, in ref 37 the adsorption at an oxygen vacancy is endergonic (+0.47 or +0.68 eV, depending on the calculation approach). The discrepancies arise most probably because supercells of different characteristics are used to model the surface, and also different approximations/computational parameters are applied. We come back to these points in relation to our findings in Section 4. We point out that from the experimental point of view, we only are aware of one work specifically devoted to study CO_2 adsorption on CeO_2 (110) surfaces, namely, the XPS/NEXAFS study of Yang et al.[42] They observe both chemisorbed and physisorbed species in the spectra, albeit as a minority species in the latter case, and this on reduced as well as on fully oxidized surfaces.

In this work, we revisit the question of the adsorption of CO_2 on a fully oxidized or stoichiometric CeO_2 (110) surface using first-principles methods. We consider all five inequivalent potentially stable adsorption sites on the (110) surface as well as different CO_2 orientations (e.g., parallel or perpendicular to the surface) at each site. We find that in almost half of the cases considered, the molecule will eventually chemisorb as a carbonate on a surface oxygen. In the rest of the cases, it will physisorb, but there are only four particular physisorption states to which the molecule will converge. To shed light on the phenomenology behind our findings, we analyze the results in the light of the CO_2 molecule energy levels, electronic structure of the surface−adsorbate system, and charge distributions. As one might expect, in the case of physisorption, the molecular energy levels as well as the surface states are relatively unperturbed. Nevertheless, we will see that the interaction is enough to cause polarization and an induced dipole moment in the CO_2 molecule, leading to its adsorption. In the case of chemisorption, on the other hand, all levels are considerably perturbed, participating directly or indirectly in the interaction. Essentially, molecular levels and surface states hybridize strongly, resulting in a carbonate species. Interestingly, the molecular nonbonding levels play a leading role in the bonding resulting in the carbonate state.

In the following section, we describe the methods and modeling used. In Section 3, we present our results, followed by a discussion in Section 4. We end the paper with conclusions in Section 5.

2. METHODOLOGY

2.1. Computational Aspects. We performed our first-principles calculations using the Vienna Ab Initio Simulation Package (VASP version 6.4.1).[43−45] We used projector augmented-wave (PAW)[46] data sets to describe core−valence interactions, as implemented in VASP.[47] More specifically, we used GW_PAWs in all cases. Because of the highly localized states arising from the Ce 4*f* orbitals, to treat the exchange-correlation energy, we adopted the PBE+*U* scheme, where PBE represents the generalized gradient approximation (GGA) functional due to Perdew−Burke−Ernzerhof (PBE).[48] For the Hubbard *U* term, we used the rotationally invariant approach of Dudarev et al.[49] Furthermore, to account for the van der Waals energy, we used the optB86b-vdW nonlocal functional.[50−52] In this approach, a nonempirical nonlocal functional is added to the correlation functional to describe the van der Waals interaction in sparse systems in general. It has been shown to provide a robust description of adsorption.[13]

Other computational specifics are as follows. The value chosen for the Hubbard *U* parameter is 5 eV. This was shown to be a good value for ceria by Nolan et al.,[53] and is the value typically used in computational studies of adsorption on ceria surfaces, such as those cited earlier.[54] The plane wave basis set energy cutoff was set at 500 eV, and total energies were converged to within 10^{-6} eV. For bulk CeO_2, a Γ-centered 6 × 6 × 6 regular **k**-point mesh is used. Its lattice parameter was determined via fitting to the Birch−Murnaghan energy-volume equation of state.[55] We find a = 5.488 Å, which is just 1.4% above the experimental value of 5.411 Å,[56] obtained from powder diffraction data[57] (see the Supporting Information for more details on this and other calculated properties of bulk CeO_2).

In its ground state, CeO_2 adopts the fluorite structure, space group $Fm\bar{3}m$ (#225). Based on our calculated lattice parameter, to model a (110) surface, we constructed a supercell consisting of a $p(2 \times 2)$ slab cut perpendicular to the [110] direction, five atomic layers thick, topped by a vacuum layer of 15 Å (see Figure 1). The purpose of the latter is to ensure a free surface model by preventing any spurious effects due to the periodicity in the direction perpendicular to the slab. For structural calculations, the corresponding Brillouin zone was sampled by a Γ-centered 5 × 7 × 1 regular mesh. As for the bulk calculations, the energy cutoff is 500 eV and total energies were converged to less than 10^{-6} eV. The structure of the surface was determined by relaxing the top three layers, keeping fixed the two bottom ones. Forces were converged to within 0.01 eV/Å using the conjugate-gradient algorithm implemented in VASP. For density of states (DOS) calculations, we used the tetrahedron method[58] and a Γ-centered 10 × 14 × 1 **k**-point mesh.

We determined the CO_2 structure and molecular orbitals using the PBE functional (in conjunction with the nonlocal van

https://doi.org/10.1021/acs.jpcc.5c01747
J. Phys. Chem. C 2025, 129, 12814−12826

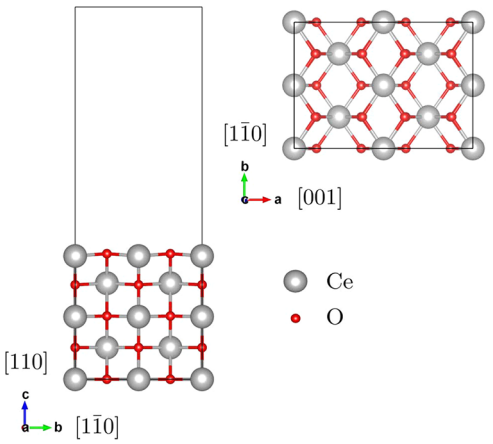

Figure 1. Slab supercell used in our adsorption calculations. The vacuum space above the slab is 15 Å high. The left side of the figure shows a side view of the supercell. Relaxation causes the top interlayer distances to contract. Contraction decreases gradually going downward. Also, the different responses of the Ce and O atoms cause a jagged behavior especially noticeable in the top layer. The right side of the figure shows a top view of the supercell.

der Waals functional discussed above, for consistency in energy comparisons). The molecule was put in a cubic box of side 12 Å for this purpose. The box is large enough that the properties determined are those of a free molecule within the accuracy of the approach used. The energy cutoff, as well as energy and forces convergence criteria were the same as for the slab calculations. The C−O bond length found is 1.173 Å, to compare with the experimental value of 1.163 Å. The difference is less than 0.9%.

Polarization was estimated using the Tkatchenko-Scheffler method with iterative Hirshfeld partitioning (Hirshfeld-I), as implemented in VASP. In this method, the original Hirshfeld partitioning method used by Tkatchenko and Scheffler[59] is replaced with the iterative procedure introduced by Bultinck et al.[60] The Hirshfeld-I method accounts better for charge polarization and redistribution, as it reflects the relative electron affinity of the atoms in a molecule, as well as the overall bonding environment. It has been shown to lead to more accurate results in systems where van der Waals interactions are important.[61,62] Charge transfers were estimated via a grid-based Bader charge analysis.[63]

A note on the figures. Crystallographic plots were made using VESTA.[64] For all other plots, including the CO_2 orbitals plots, we used Matlab.[65]

2.2. Adsorption Geometries. In Figure 1, we show a side view and a top view of the supercell used to model the surface. We adjoin to the supercell axis labels the corresponding directions in the fluorite structure. The layers are stoichiometric, so the surface is charge neutral. Relaxation causes the upper interlayer distances to contract, a phenomenon common to other fluorite oxides surfaces, such as UO_2.[66] The contraction of the subsurface layers decreases gradually. Also, the Ce atoms respond more strongly to relaxation than the O atoms, in line with what Nolan et al. report,[53] causing the Ce−O layers to slightly split. This is the reason for the jagged appearance of the upper Ce−O layers in Figure 1, especially in the top layer. See Supporting Information for detailed data on the interlayer distances.

In Figure 2a, we show a top view of the supercell, indicating the five inequivalent potentially stable adsorption sites considered in our study. For clarity, the atoms in the subsurface layer are shown in faded colors, acknowledging that their direct effect on adsorption can be expected to be considerably weaker than the effect of the top layer atoms. The Ce atoms in the subsurface layer are ∼1.7 Å below the top layer Ce atoms, and the O atoms in the same subsurface layer are ∼1.9 Å below the top layer O atoms.[67] In the figure, we show the label used for each site. The abbreviations used hereafter for simplicity are——Diamond-hollow: dh; O-top: ot; O−O bridge: oo; Hexagonal-hollow: hh; Ce-top: ct. Notice that except for the O-top, the sites coincide with high-symmetry lattice points. Further down, we will see that it is

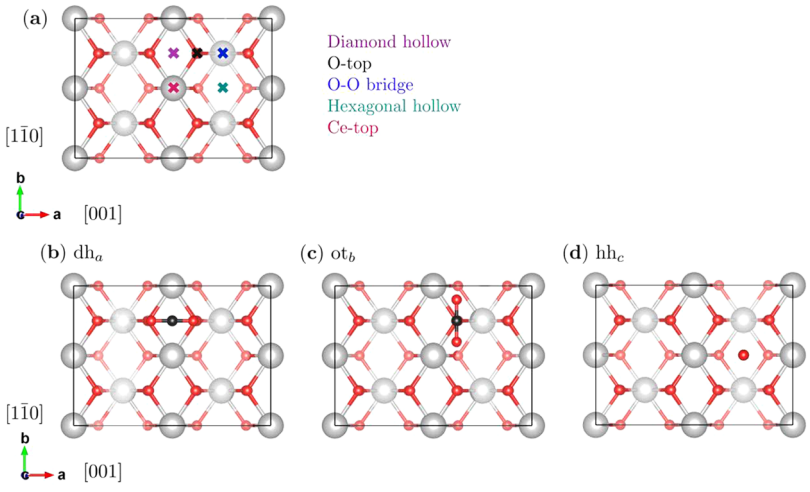

Figure 2. Adsorption sites and CO_2 molecule orientations. The carbon atom is colored black. (a) Top view of the slab supercell showing the possible CO_2 adsorption sites considered in this work. The atoms in the subsurface layer are shown in faded colors for clarity. Site names and abbreviations are as follows——Diamond-hollow: dh; O-top: ot; O−O bridge: oo; Hexagonal-hollow: hh; Ce-top: ct. (b) Molecule along the **a**-direction ([001]) at the Diamond-hollow site: dh$_a$. (c) Molecule along the **b**-direction ([1$\bar{1}$0]) at the O-top site: ot$_b$. (d) Molecule along the **c**-direction ([110]) at the Hexagonal-hollow site: hh$_c$. In all cases, the molecule is placed at a height of 2.6 Å above the top oxygen atoms plane. The reference atom in the molecule for this is the carbon atom in panels (b) and (c) and the bottom oxygen atom in panel (d).

https://doi.org/10.1021/acs.jpcc.5c01747
J. Phys. Chem. C 2025, 129, 12814−12826

important to take this into account when running the calculations.

The CO_2 molecule is linear; therefore, for the adsorption calculations, it can be set in three main orientations with respect to the surface. Referring to Figure 1, these are the [001], [1$\bar{1}$0], and [110] CeO_2 fluorite structure directions, or equivalently, the **a**, **b**, and **c** supercell axis directions. Thus, in the first two cases, the molecule lies parallel to the surface, and in the latter case, it is perpendicular to it. Taking the results of previous works as a guide,[27,28] we chose to always set the CO_2 molecule initially at a height of 2.6 Å above the plane of the top oxygen atoms. Specifically, when the molecule is parallel to the surface, it is the carbon atom that is the reference for this. That is, it is the carbon atom that lies directly above the site considered at the height indicated. When the molecule is perpendicular to the surface, it is the lower oxygen atom that is the reference atom. To simplify the notation, the orientation of a molecule at a given site is indicated by a subindex. A molecule initially set at site Diamond-hollow (dh) oriented parallel to the *a* axis is said to be set in the dh_a geometry. A similar convention applies to the initial orientation in the other directions, i.e., along [1$\bar{1}$0]: subindex *b*; along [110]: subindex *c*. In panels (b–d) of Figure 2, we present an example for each one of the three cases. In this work, we consider, thus, 15 initial geometries.

3. RESULTS

3.1. CO_2 Molecular Orbitals and Energy Levels. For a closer analysis of the interaction of the CO_2 molecule and the CeO_2 surface, it is important to know what the energy spectrum of the molecule is, in comparison with the electronic structure of the surface. For completeness and for further reference in this work, we show in Figure 4 the free molecule energy levels we computed and the associated orbitals. The latter are readily obtained using the wave function expansion coefficients in the WAVECAR file output by VASP. Our calculated valence energy levels correlate very well with the X-ray photoelectron spectroscopy results of Allan et al.[68] The lowest occupied orbital is the $3\sigma_g$ and the highest occupied orbitals (HOMO) are the $1\pi_g$, with a total valence spectrum width of ∼20 eV, matching very well experiment. The width of the upper part of the spectrum (∼4.7 eV: $4\sigma_g$–$1\pi_g$) is rather close to experiment as well. Also, in ref 68, it is deduced that the lowest unoccupied molecular orbital (LUMO) is the $5\sigma_g$, in coincidence with what we find.[69] Note that the measurements reported are not able to resolve the splitting between the $3\sigma_u$ and $1\pi_u$ orbitals in the valence band. Based on the self-consistent molecular orbital computational methods available at the time, Allan and co-workers tentatively designate the $3\sigma_u$ to be lower. Our calculations indeed predict nearly degenerate energies, but we find the reverse ordering, as shown in Figure 3. Of course, this has little effect on the molecule total energy. In any case, we shall see later that this ordering does not play an important role with regard to the CO_2 adsorption cases we consider. Finally, Allan et al. suggest that the orbital lying above the LUMO is $4\sigma_u$, with the two $2\pi_u$ orbitals lying higher up in energy. We find it to be the reverse, as shown in Figure 3. Again, this is of no consequence to our analysis further down as these energy levels lie above the CeO_2 surface calculated conduction band minimum and do not contribute to adsorption. It would be interesting, nonetheless, to have more recent experimental results on the CO_2 molecular energy levels.

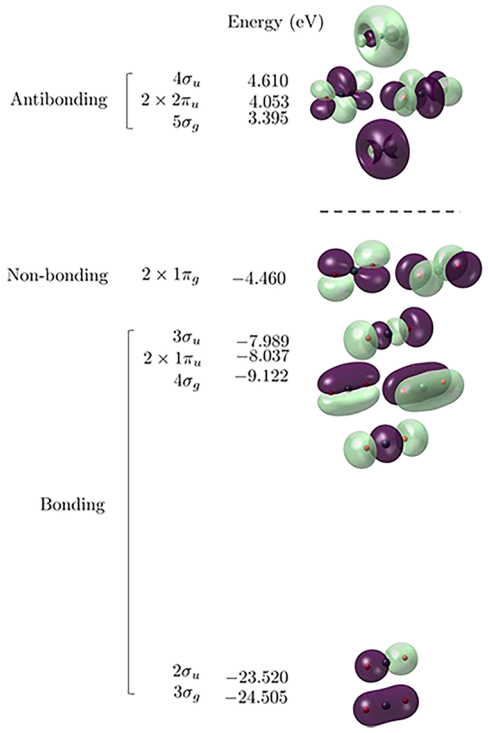

Figure 3. Calculated CO_2 energy levels and molecular orbitals. The plots show the orbital amplitudes times the sign of the phase of the corresponding wave function; the color indicates the sign (purple: positive, light green: negative). The isosurfaces are such that 90% of the charge is enclosed by them, except in the case of $5\sigma_g$ and $4\sigma_u$, for which it is 70% for visualization purposes. The dotted line separates the occupied and unoccupied orbitals; i.e., the HOMO states are the $1\pi_g$ and the LUMO the $5\sigma_g$. Notice the large energy gap between these levels.

3.2. Physisorption and Chemisorption. The adsorption energies were calculated as $E_a = E_{[110]\ \text{slab}\ +\ CO_2} - E_{[110]\ \text{slab}} - E_{CO_2}$. Here, $E_{[110]\ \text{slab}\ +\ CO_2}$ is the total energy of the slab + CO_2 molecule system. This is calculated after a full relaxation of the molecule and again the upper three atomic layers of the slab. $E_{[110]\ \text{slab}}$ and E_{CO_2} represent the total energies of the relaxed free slab and free CO_2 molecule, respectively. Starting from the 15 geometries indicated above, we found that there are in all only five stable adsorption states. Their characteristics are listed in Table 1. The adsorption states labels in the first column indicating their location and orientation follow the same convention as for the initial geometries. To avoid confusion between the adsorbed state label and the initial geometry label, we added a superscript (^{a}, for "adsorbed") to the former. The last column in Table 1 indicates which initial geometries lead to the corresponding adsorbed state. The five stable adsorption states are depicted in Figure 4. The adsorption energies in the second column of Table 1 very strongly suggest adsorption either by physisorption or by chemisorption. Indeed, in physisorption adsorption energies typically range from 10 to a few hundred meV, while chemisorption adsorption energies are typically larger than 1 eV.[15,20,70] The reason for the low adsorption energies in physisorption is that it is governed by van der Waals interactions. It consists of the Pauli repulsion in the short-range and the comparatively weak polarization or dispersion forces at long range. This results in general in a shallow

https://doi.org/10.1021/acs.jpcc.5c01747
J. Phys. Chem. C 2025, 129, 12814–12826

Table 1. CO_2 Adsorption Energies (eV) on CeO_2 [110], Heights above the Surface, C−O Bond Lengths, and O−C−O Angle[a]

state	E_a (eV)	H (Å)	l_{C-O} Å	$\angle_{O-C-O}$ (°)	initial geom.
dh_b^α	−0.551	2.5	1.176	173.9	dh_b, dh_c, ct_b
ot_b^α	−1.765		1.278(2),1.347	116.4(2),126.7	dh_a, ot_a, ot_b, ot_c, oo_a, oo_c, hh_b
oo_b^α	−0.514	2.2	1.177	171.2	oo_b
hh_a^α	−0.549	2.4	1.173	177.0	hh_a, hh_c, ct_a
ct_c^α	−0.266	2.8	1.173,1.170	180.0	ct_c

[a]The height is relative to the closest oxygen in the topmost oxygen plane. The CO_2 molecule is bent to different degrees. Bond lengths are also affected differently. In the ot_b^α case, the adsorbed molecule forms a carbonate species with a top oxygen atom, so there are three C−O bonds. The (2) in the corresponding entries means that two bond lengths and two angles share the same value.

attractive potential. When trapped, the adsorbate retains its chemical species and does not attach chemically to the surface. On the other hand, in chemisorption, the adsorption energies are larger, of the order of chemical bonding energies, because a chemical bond is formed between the adsorbate and the surface. Hence, as can be expected, there are clear changes in the structure and energy levels of the adsorbate and the surface that correlate directly with the resulting adsorption energy. Our analysis in the next subsection, based on the surface electronic structure and energy levels of the molecule of three representative cases, corroborates this.

According to the adsorption energies in Table 1, there are four physisorption states and one chemisorption state. Specifically, each of the high-symmetry locations (Figure 2) harbors a physisorption state, while the chemisorption state occurs at the O-top site. Table 1 further shows that whether physisorption or chemisorption occurs is highly dependent on the initial orientation of the molecule relative to the surface, as well as on the site approached. Furthermore, in several cases, the CO_2 molecule will be drawn to move toward a neighboring site and/or rotate until finally physisorbed or chemisorbed. Thus, 8 out of the 15 initial geometries considered lead to one of the four physisorption states. The energies suggest moderate (ct_c^α) and strong (dh_b^α, oo_b^α, and hh_a^α) physisorption. Except for the ct_c^α case, the molecule is slightly bent in the physisorbed states. In the ct_c^α case, the molecule remains essentially linear, but the C−O bond lengths are slightly different. Table 1 also shows that remarkably, all seven remaining initial geometries lead to the ot_b^α chemisorbed state. Its adsorption energy of −1.765 eV clearly falls in the chemisorption range. As will be illustrated in the next subsection, the CO_2 molecule forms a carbonate species with the surface oxygen. The bond length of 1.347 Å given in Table 1 corresponds to the carbon atom−surface oxygen bond length. In forming the carbonate, the CO_2 molecule pulls upward the surface oxygen atom by 0.274 Å; it also displaces it in the direction of the **a** axis by 0.165 Å (see Figure 4; the upward displacement is clearly seen, but the **a**-direction displacement is less discernible). Note also that the bond angles and bond lengths in Table 1 indicate that the carbonate deviates from trigonal planar symmetry. It is slightly tetrahedral because of the interaction with the surface.

Let us point out that taking into account the site multiplicity due to the symmetry of the surface, as well as the initial molecule orientations, the actual ratio of initial geometries or configurations leading to chemisorption to those leading to physisorption is 5:4. Note also that our calculations do not take into account temperature effects, but in experiments, these can be important. In particular, it is known that physisorption generally decreases with temperature. For instance, the actual adsorption energy can be weaker due to vibrational energy. On the other hand, chemisorption benefits from temperature if it is not too high, as it can provide the necessary activation energy

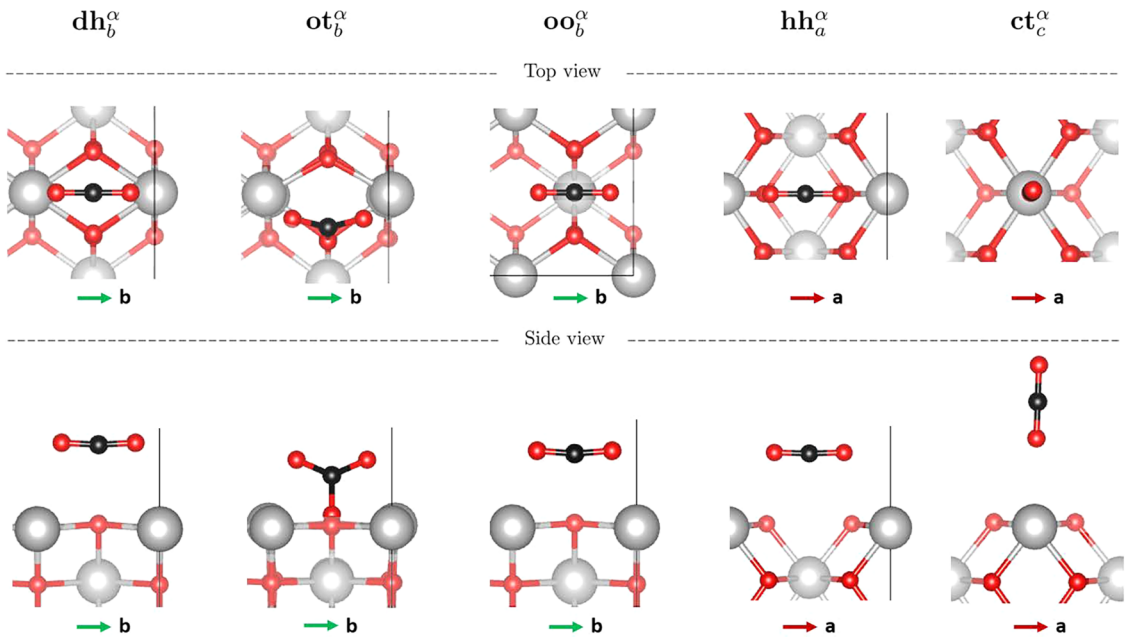

Figure 4. Five stable adsorption states found in this work. States dh_b^α, oo_b^α, hh_a^α, and ct_c^α are physisorbed states; ot_b^α is a chemisorbed state. The latter is a carbonate species; notice that the surface oxygen atom participating in it is pulled upward. The slight bending of the CO_2 molecule in states dh_b^α, oo_b^α, and hh_a^α indicates an induced dipole moment. State ct_a^α presents a dipole moment as well, but it is essentially linear. The colored arrows refer to the supercell axes (see Figure 2). The view in the top row plots is from the above. In the bottom row, the vertical axis is the **c** axis.

https://doi.org/10.1021/acs.jpcc.5c01747
J. Phys. Chem. C 2025, 129, 12814−12826

for bond formation. Thus, with increasing temperature, the chemisorption to physisorption ratio can be expected to be higher. In this sense, our results point in the same direction as the experimental findings of Yang et al.[42] Indeed, in their XPS/EXAFS study, they observe that CO_2 adsorbs mainly as a carbonate on fully oxidized CeO_2 (110), and only physisorbs as a minority species.

We call attention to the following regarding the calculation of the adsorption state in the neighborhood of a high-symmetry site. If the initial position of the CO_2 molecule is exactly on-site in a high-symmetry location, it will not necessarily relax to the corresponding lowest energy adsorption state. The reason for this is that the total electrostatic force on a charge located in such a symmetric position is zero. The CO_2 molecule is not a point charge but is linear and symmetric with respect to the carbon atom. Even if symmetry is disabled in the calculations (`ISYM = 0` in VASP), the site symmetry will be reflected in the forces acting on the molecule. Thus, relaxation in such a setting sometimes leads to a metastable state. For instance, setting the CO_2 molecule exactly in the hh_c geometry, it will come to rest at a height of 2.2 Å directly below the initial point, keeping its vertical orientation. The calculated adsorption energy would then be −0.141 eV, but the state is not stable. Restarting the calculation after perturbing the molecule position slightly, i.e., moving it ∼0.2 Å in a diagonal direction to break the unintended symmetry effects, results in the molecule evolving further, reorienting itself parallel to the surface and finally falling into the much lower energy state indicated in Table 1 (note that the molecule moves away from the surface). To avoid such problems, it is enough to locate the CO_2 molecule initially slightly off-site. Of course, if indeed a locally stable adsorption state preserving the initial orientation can be found at a high-symmetry location, then the molecule will still be driven to it (as implicitly shown in the table). For completeness and for the purposes of comparison, we carried out the calculations for all 15 cases considered in this work starting from the on-site settings as well (same initial height as for the off-site calculations). The adsorption data for these cases are given in Table S1 in the Supporting Information.

To close this subsection, we point out that the above shows that the five adsorption states identified exhaust all of the stable adsorption sites. Indeed, if the CO_2 molecule is initially set at an intermediate location between those considered above, it will be in the basin of attraction of one or the other adsorption state, and will eventually converge to it. In the following subsection, we look at the insight on adsorption that can be gained by comparing the energy structure and energy levels of the clean slab, the free molecule, and the surface−adsorbate system, as well as the charge distribution in them. We consider three representative adsorption cases among the above.

3.3. Electronic Structure and Charge Distribution. As suggested in the previous subsection, the adsorption energies in Table 1 can be roughly classified as moderate physisorption, strong physisorption, and chemisorption. As representative of each case, we analyze below the phenomenology behind the adsorption states ct_c^α, dh_b^α, and ot_b^α.

3.3.1. Moderate Physisorption. Prior to our analysis, we note that compared to the bulk, the slab Ce 5*s* energy levels are split because the Ce atoms in different layers are inequivalent. Also, the bandwidths are larger than those of the bulk. This is due to the contraction of the upper Ce−O layers that was discussed before. Such an effect on bandwidths due to contraction is well-known in insulating or semiconducting materials[71] (see the Supporting Information for more details on the bulk-slab electronic structure comparison).

Now, an electronic structure comparison requires a common energy reference. Since the Ce 5*s* levels of the free slab are quite deep in energy, one can expect that they will not be significantly affected by the adsorbed molecule and can be used for that purpose. We begin by considering the ct_c^α adsorption state, for which the adsorption energy is moderate in comparison with those of the other physisorption states (see Table 1). In Figure 5a, we plot simultaneously the DOS

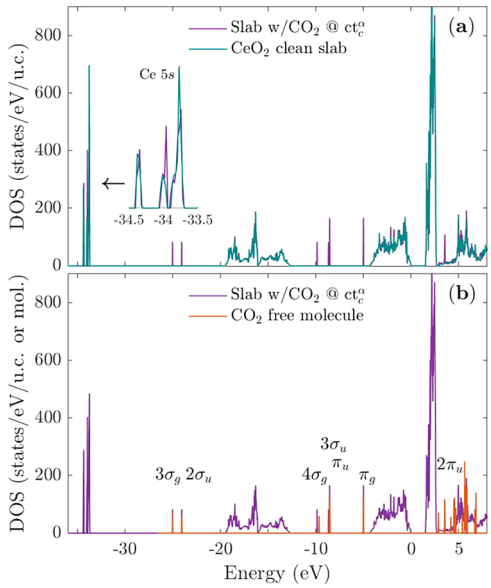

Figure 5. (a) DOS of the CeO_2 clean slab and of the slab with the molecule adsorbed in the ct_c^α state above a Ce atom, aligned according to the lowest Ce 5*s* levels. The main difference comes from the CO_2 levels in the slab with the molecule adsorbed. Otherwise, although real, the difference is small. (b) Plot overlapping the DOS of the slab with the adsorbed molecule and the free CO_2 molecule levels. The peaks corresponding to CO_2 in the former can be readily identified thanks to *spd*- and site projections. The adsorbed molecule is very weakly perturbed but enough to lead to an induced dipole moment and physisorption.

corresponding to that case and of DOS of the clean slab, aligning their Ce 5*s* levels.[72] The inset in the figure is an enlargement showing the close alignment of the Ce 5*s* manifold of the two spectra. One immediately notices a series of narrow peaks in the spectrum of the slab with CO_2 adsorbed, absent in the spectrum of the clean slab. Obviously, these peaks are due to the adsorbed molecule. Aside from this, the alignment leads to nearly perfect overlap of the CeO_2 levels. Notably, the bandwidths and the valence band maximum (VBM) of both spectra coincide. Note, however, that at certain energy values, there is a slight difference in intensity, for instance, in the [−5,0] eV energy interval.

Going back to the peaks due to CO_2, we looked at the *spd*-projection data to determine the character of the corresponding states. Remarkably, these were found to be of pure CO_2 character, with a clear one-to-one correspondence with the levels of the free molecule. The character of the levels is corroborated in the energy band plot corresponding to this state; see Supporting Information. To study more closely the effects on the adsorbed molecule levels due to the interaction with the slab, in Figure 5b, we overlaid the energy level

https://doi.org/10.1021/acs.jpcc.5c01747
J. Phys. Chem. C 2025, 129, 12814−12826

spectrum of the free CO_2 molecule on top of the DOS of the slab with the adsorbed CO_2 molecule. The labels indicate the orbital character of the peaks due to the adsorbed molecule.[73] The $3\sigma_g$ peaks were used to align the two spectra. The degeneracies of the π_u, π_g, and $2\pi_u$ levels of the CO_2 molecule in the slab are very slightly lifted (recall the degeneracies shown in Figure 3). The differences are of the order of the meV and so not resolved in the plot. It is also quite significant that the relative differences in energy levels appear to be relatively weakly affected by the interaction with the slab. Nevertheless, the $4\sigma_g$ level is shifted noticeably downward, and, moreover, the $3\sigma_u$ and π_u levels present a reversed order compared to the free molecule. In any case, as the *spd*-projection and band structure analyses show, the ground state levels of the molecule remain fully occupied. As can be expected, a Bader charge analysis shows that the total charge of the CO_2 molecule remains unchanged (see the Supporting Information). This implies that there is no charge transfer between the molecule and the surface and no chemical bond. On the other hand, at the equilibrium position, the interaction between the molecule and the surface leads to a change in the polarization of the CO_2 molecule. Indeed, a Hirshfeld-I calculation shows that the carbon and upper-lying oxygen atoms become more positive (+0.073*e* and +0.004*e*, respectively),[74] while the lower oxygen atom becomes more negative (−0.112*e*). Hence, although the molecule remains essentially linear (Table 1), it presents an induced dipole moment. By the same token, the surface atoms are subject to a slight polarization mutation, reflected in the slight changes in the surface density of states mentioned before; in particular, the Hirshfeld-I charges show that the Ce atom below the molecule becomes more positive (+0.040*e*).[75] Therefore, the adsorption mechanism can be seen as follows. An equilibrium height of 2.8 Å (see Table 1) means that the molecule has been pushed away from the surface, as the initial height was 2.6 Å. Thus, initially, the dominant force is the short-range Pauli repulsion. Thereafter, the molecule reaches equilibrium owing to the polarization of the surface and the induced dipole in the molecule.[76] Thus, the interaction can be seen as a Debye type of van der Waals interaction, where the attractive forces are essentially due to induced polarization.[13,40]

3.3.2. Strong Physisorption. We now consider the dh_b^α adsorption state. With a −0.551 eV adsorption energy, it is in a strong physisorption class. Figure 6a shows, similar to the previous case, the DOS of the clean slab and of the slab with the adsorbed molecule aligned, as determined by the lowest Ce 5*s* level (not shown explicitly in the figure). Again, bandwidths are conserved and result in coincident VBMs. As in the previous case, the DOS shows some slight intensity differences, signaling some charge distribution changes. The effect of the interaction on the CO_2 levels is similar to what was observed in the ct_c^α case, only stronger. In Figure 6b, the free molecule levels are plotted on top of the DOS of the slab with the molecule adsorbed (here, too, the $3\sigma_g$ levels are used to align the spectra). With respect to the two lowest levels, which conserve their relative energy difference, the $4\sigma_g$ level is shifted, as in the ct_c^α case. The order of π_u and $3\sigma_u$ is also inverted with respect to the free molecule. The degeneracy of the π_u and π_g levels is lifted as in the previous case, but only more markedly. This is more obvious in the π_g case in Figure 6a. Similarly, the $2\pi_u$ degeneracy is visibly lifted [this is also more clear in Figure 6a]. There is no significant hybridization of the CO_2 levels with the CeO_2 surface states, and the affected ground state levels of

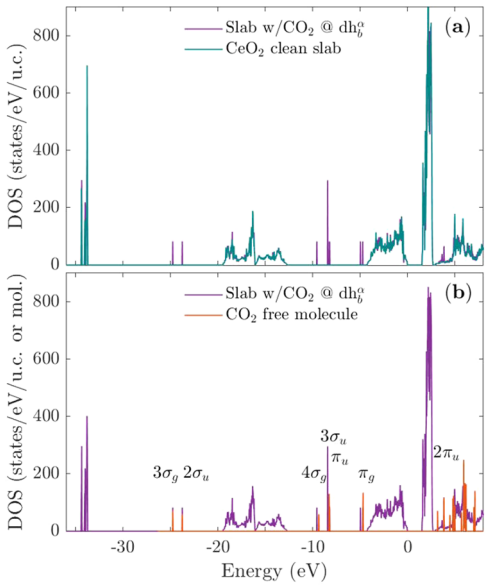

Figure 6. (a) DOS of the CeO_2 clean slab and of the slab with the molecule adsorbed in the dh_b^α state above a Diamond-hollow area, aligned according to the lowest Ce 5*s* levels, as in the previous case. Here, the effects of the molecule−surface interaction are more noticeable, in the intensities of both the slab and of the molecule. (b) Plot overlapping the DOS of the slab with the adsorbed molecule and of the free CO_2 molecule. The degeneracy of π_u and π_g is more markedly lifted, and the order of the π_u and $3\sigma_s$ levels is inverted. In this case, the molecule bending associated with the induced dipole moment is stronger, and so is the physisorption.

the molecule remain fully occupied. A Bader analysis again shows basically no charge transfer between the CO_2 molecule and the surface (see the Supporting Information). That the interaction is stronger here than in the moderate physisorption case is manifested in two ways. First, the molecule shows greater polarization. Indeed, the Hirshfeld-I charges show that carbon becomes more positive by +0.144*e* and the oxygen atoms become more negative by −0.105*e* each. In addition, there is bending of the molecule (173.9°), which certainly translates into a stronger induced dipole moment. Second, because of the interaction, both the Ce atoms closest to the molecule oxygen atom show an increase in polarization; the Hirshfeld-I charges show that they become more positive by +0.028*e* each. Note that the molecule equilibrium position is 2.5 Å above the surface; i.e., it is drawn closer to the surface, lower than in the previous case (2.8 Å, taking as reference the lower oxygen atom). This can also be seen as reflecting a stronger force, which generally correlates with the height above the surface at which a physisorbed molecule reaches equilibrium. Again, the net effect is that the CO_2 molecule reaches equilibrium through the interplay between the surface polarization and the induced dipole moment in the molecule. Hence, also in this case, the physisorption can be considered of Debye type.

Let us add here that the same can be concluded about the two other strong physisorption cases, oo_b^α and hh_a^α. Although the adsorption energies, bond lengths, and bending angles are somewhat different, the phenomenology is essentially the same.

3.3.3. Chemisorption. We turn now to the chemisorption case, the ot_b^α state. In Figure 7a, we show the DOS plots of the clean slab and the slab with the adsorbed CO_2 molecule,

https://doi.org/10.1021/acs.jpcc.5c01747
J. Phys. Chem. C 2025, 129, 12814−12826

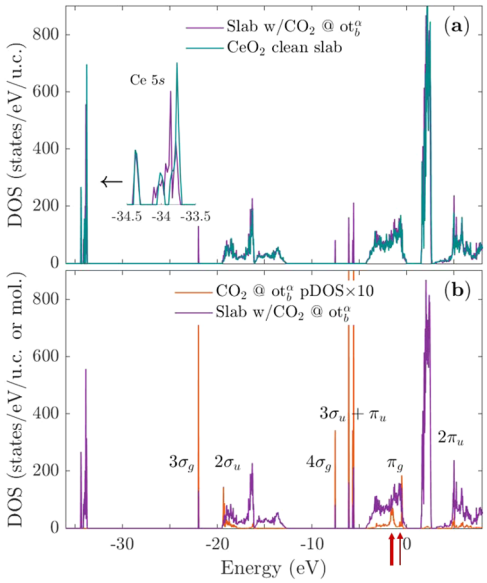

Figure 7. (a) DOS of the CeO_2 clean slab and of the slab with the molecule adsorbed by a top oxygen in an ot_b^α state, aligned according to the lowest Ce 5*s* levels, as in the previous cases. The inset shows the alignment and at the same time that the upper Ce 5*s* levels are strongly perturbed. Also, the levels arising from CO_2 appear very different from those of the free molecule. (b) Plot overlapping the DOS of the slab with the adsorbed molecule and of the projected adsorbed CO_2 DOS. The latter is multiplied by 10 for the sake of clarity. All CO_2 levels present hybridization with slab states, but it is particularly clear in the case of the $2\sigma_u$ and π_g levels. The $3\sigma_u$ and π_u levels give rise to mixed states peaks. An analysis of the DOS data shows that not only the π_g hybridize with the slab O 2*p* states, but the σ_g and the π_u, and $3\sigma_u$ as well. The hybridization signals bond formation. (The meaning of the red arrows is explained below in the discussion of Figure 8).

aligned according to the lowest Ce 5*s* level, as in the preceding cases. The DOS of the slab with the adsorbed molecule presents substantial differences compared with the two preceding cases. Although bandwidths and VBM remain remarkably the same, the contribution to the DOS of the states due to CO_2 is quite different from those in the physisorption cases. As the inset shows, the splitting of the reference Ce 5*s* levels is no longer preserved. Furthermore, the number of distinct peaks due to CO_2 is not the same as in the physisorption cases, and the energy spectrum of the free molecule does not seem recognizable anymore. Also, the DOS intensity changes in the upper valence band are more important. To understand this better, in Figure 7b, we show the DOS of the slab with the adsorbed CO_2 in the ot_b^α state, overlapped with the projected DOS of the adsorbed molecule (multiplied by 10 for clarity). There is obviously a much stronger interaction between the CO_2 levels and slab states. Thanks to the *spd*- and site projection, it is still possible to identify the main character of the states arising from the CO_2 levels. These are strongly shifted upward compared to their value for the free molecule if the Ce 5*s* levels are used as a guide. Quite significantly, in contrast to the physisorption cases, they all have some level of hybridization with CeO_2 states. It is especially strong in the cases of the $2\sigma_u$ and π_g levels. The $2\sigma_u$ is pulled into the bottom of the lower CeO_2 slab valence band and spread out because of the hybridization with the slab O 2*s* and Ce 5*p* levels. The $4\sigma_g$, π_u, and $3\sigma_u$ are also hybridized with the slab O 2*p* levels while conserving to an extent their original orbital character. But as suggested in the figure, the latter two give rise to three mixed states (recall that the π_u are originally doubly degenerate). The π_g degeneracy is lifted and the split levels are largely hybridized with the slab O 2*p* levels. The outcome of these interactions is that a bent CO_2 forms a carbonate species with a surface oxygen, as shown in the plots in Figure 8. These plots show the charge associated with the states in two narrow energy windows around the two π_g peaks in Figure 7b. The red arrows in Figure 7b point to the energy windows, their thickness indicating qualitatively their width. Figure 8a corresponds to states giving rise to the sharp peak just below the VBM, indicated by the thin arrow (66 meV window), and Figure 8b corresponds to the states giving rise to the broader peak roughly 1 eV below, indicated by the thicker arrow (340 meV window). The outer lobes arise mainly from the 2*p* levels of the molecule oxygen atoms (π_g), while the lower lobes arise mainly from the hybridized surface oxygen 2*p* levels. The stronger hybridization associated with the broader peak is evident in Figure 8b, as the corresponding charge is shared by the surface oxygen atoms. This is weaker in Figure 8a. The binding to the surface is monodentate, as is reflected in the plots. Analysis of the projected DOS indeed shows negligible contribution to hybridization from the Ce atoms, as

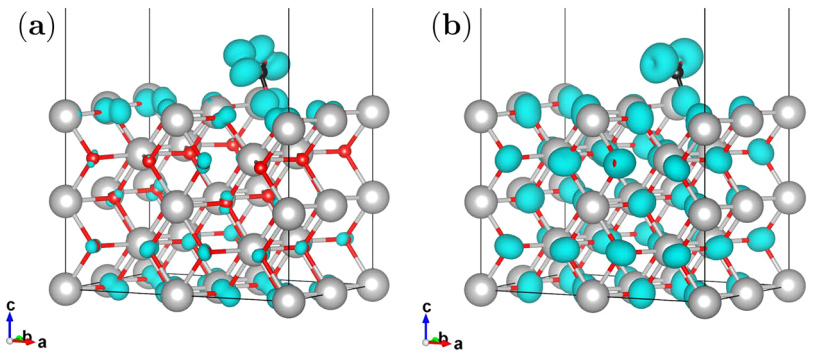

Figure 8. (a) Charge density associated with the states around the narrow peak just below the VBM indicated by the thin arrow in Figure 7(b). It shows the lobes arising mainly from the π_g levels of the molecule, but also the charge due to the 2*p* states of the slab oxygen atoms. The carbonate species is clearly identifiable. (b) Charge density associated with the states around the broader peak, indicated by the thicker arrow in Figure 7(b), which arises mainly from hybridization of the π_g levels and the surface O 2*p* states. This leads again to a clearly identifiable carbonate species, but the interaction with the slab oxygen 2*p* states is much more extended. Note that the default VESTA isosurface values were applied, which in the present case means that roughly 50% of the charge is enclosed by the isosurfaces.

https://doi.org/10.1021/acs.jpcc.5c01747
J. Phys. Chem. C 2025, 129, 12814−12826

Table 2. CO_2 Adsorption Energies (eV) on CeO_2 [110] Using Different Methodologies[a]

init. height above surface			Grimme method			slab model		
ads. energy (eV)			ads. energy (eV)			ot_b^α ads. energy (eV)		
H (Å)	dh_b^α	ot_b^α	method	dh_b^α	ot_b^α	cell size	5 layers	7 layers
2.6	−0.5513	−1.7653	DFT-D2	−0.6212	−1.6673	$p(2 \times 2)$	−1.7653	−1.7605
3.0	−0.5512	−1.7653	DFT-D3[a]	−0.4150	−1.5630	$p(3 \times 3)$	−1.8784	−1.8706
3.5	−0.5514	−1.7650	DFT-D3[b]	−0.4675	−1.6287	$p(4 \times 4)$	−1.9092	−1.9063

[a]The left side presents the energies for the dh_b^α and ot_b^α states obtained by setting the molecule initially at different heights above the surface. The data at the center present the adsorption energies obtained using different Grimme methods to account for the van de Waals interaction; D3[a] stands for zero damping and D3[b] for Becke-Johnson damping. The right side data present the ot_b^α adsorption energies for supercells of different sizes and slabs 5 and 7 layers thick.

compared to the dominant surface oxygen atoms contribution. Applying a Bader charge analysis to the carbonate ion, one can estimate the charge transfers involved in its formation. The surface oxygen atom in the carbonate is more negative by $-0.024e$, compared to its charge in the clean surface. The carbon atom is more positive by $+0.110e$, and the oxygen atoms coming from CO_2 are more negative by $-0.170e$ each, compared to their charge in the free CO_2 molecule.

4. DISCUSSION

Let us begin by discussing the differences between our results and those of previous computational studies. We first briefly address works that neglect the van der Waals interaction altogether. In ref 27, Cheng et al. report that CO_2 will only physisorb on stoichiometric CeO_2 (110) surfaces. While they do find physisorption states similar to the ones we report in Table 1, there are quantitative differences. In particular, the adsorption energies are systematically underestimated in comparison with our results. Moreover, they fail to find any chemisorption state involving a top surface oxygen. Let us also mention the work of Kumari et al.,[28] who report what is basically the dh_b^α physisorbed state we discussed in the previous section. The adsorption energy they find is considerably weaker than what we find, −0.243 vs −0.551 eV in our case. Similarly, no chemisorption state is reported. The discrepancies can be understood as due to the omission of the van der Waals interaction in those works. It is known that calculations omitting that interaction tend to systematically underestimate adsorption energies.[13,77−79] Functionals accounting for the van der Waals interaction not only improve the stability of physisorption states. It has been shown, in particular, that they can correctly stabilize chemisorption states where standard functionals, such as GGA, predict only weak physisorption.[13,77]

Among the first reports on CO_2 adsorption on CeO_2 (110) taking into account the van der Waals interaction, there is the work of Kumari et al. in ref 30. In it, they recalculate the adsorption energy for the dh_b^α state reported in their previous work.[28] It is indicated that for the van der Waals interaction, a Grimme model is used, though without further details (there are various Grimme-type models that are used in the literature). Surprisingly, the recalculated adsorption energy is weaker than in their previous report, −0.197 vs −0.243 eV. The main reason for the unexpected result is probably the too thin slab used to model the CeO_2 surface. Indeed, they use a three-atomic-layer slab, fixing the two bottom layers during relaxation. This is unlikely to yield a properly relaxed surface and a correct adsorption state.

The chemisorbed state ot_b^α we find is also reported in the work of Symington et al.[34] The main methodological difference with our work appears to be that they use a seven-layer slab to model the surface. We verified, however, that a seven-layer model essentially corroborates our results (see Table 2 further down). The main results reported by those authors are obtained without including the van der Waals interaction in their calculations. The adsorption energy they thus find for the chemisorbed state is −1.32 eV, so somewhat weaker than what we find (−1.765 e V). They indicate that they performed a calculation for this case including the van der Waals interaction,[80] which yielded an adsorption energy differing from their first result by +0.07 eV, a surprisingly small difference. Intriguingly, moreover, they indicate that the binding to the surface is tridentate, with the molecule oxygen atoms bound to the nearest surface Ce atoms. The reason for the discrepancy with our findings is not clear to us, but we do not find support for this. Not in the *spd*-analysis of the adsorbed molecule oxygen atoms states, nor in the overall charge density. We note that Symington et al. state that the tridentate state is also the favored state on the CeO2 (111) surface. This is in contradiction, however, with the findings of Hahn and co-workers, who studied the same case and found that monodentate adsorption is the one that is energetically more favorable on that surface.[81]

Zhu et al. report an adsorption energy of −0.787 eV for the chemisorbed state,[35] which represents a considerably weaker binding than what we find. They used for their calculations a four-layer slab to model the surface, fixing the positions of the two lower layers for the relaxation calculations. In our view, relaxing only two layers is still not enough to simulate a free surface. The supercell used appears to be a $p(2 \times 4)$ cell. The energy cutoff used in their work is lower than what we use (450 eV vs 500 eV), and they indicate that the van der Waals interaction is accounted for using what we understand is one of the Grimme atom-pairwise summation methods implemented in VASP (it is only specified that a D3 method is used), but it is not certain to what extent this contributes to the difference with our results. We also mention that Zhu et al. indicate that the adsorption they find is of "M-type". There is no direct clarification as to what this entails, but the figure provided by those authors suggests that they are referring to a tridentate binding, as in the work of Symington et al. As indicated above, this is not supported by our findings.

In the work of Gao et al., CO_2 is found to chemisorb on a surface top oxygen with an adsorption energy of −0.32 eV. This is quite a weak energy for chemisorption. Unfortunately, few details are given as to the model used.[36] It appears that a $p(2 \times 2)$ supercell is used, but the thicknesses of the slab and of the vacuum space above it are not indicated. The van der Waals interaction is included in their calculations using the Grimme DFT-D3 method implemented in VASP. The energy

https://doi.org/10.1021/acs.jpcc.5c01747
J. Phys. Chem. C 2025, 129, 12814−12826

cutoff is somewhat too low (400 eV), and the calculations are single-point (Γ point). The Hubbard U parameter value used is 4.5 eV. While they do find that the CO_2 binding to the surface oxygen is monodentate, the molecule is rotated 90° with respect to what we and the works above find. Indeed, according to Figure 5, the CO_2 molecule is roughly parallel to the [001] direction, instead of the $[1\bar{1}0]$ direction (see Figure 2). We note that a physisorbed state is reported that is quite similar to the hh_a^{α} state we find, but the adsorption energy is much weaker, −0.250 vs −0.549 eV.

Finally, let us address the work of Keller et al.[37] As in the work of Gao et al. just discussed, these authors find that the molecule chemisorbed to a top oxygen atom is rotated by 90°. In addition, they suggest that the binding is bidentate, as they indicate that one of the molecule oxygen atoms interacts with the neighboring surface Ce atom. We already mentioned that we do not observe any significant Ce-molecule oxygen interaction. The adsorption energy reported by Keller and co-workers is stronger than in ref 36, −0.84 eV (−0.81 eV without including a Hubbard U), but still considerably weaker than what we find. In their work, Keller et al. also considered the adsorption of CO_2 on the top oxygen vacancy. Strangely, they find a positive value of +0.68 eV (+0.47 eV without Hubbard U). This is in contradiction with all of the previous works that have considered such an adsorption on CeO_2 (110) surfaces. The adsorption in the latter case is typically found to be not only negative, but in fact stronger than the adsorption on a top oxygen.[30,34,35] This is also what is suggested by the experimental results of Yang et al.[42] Let us just mention that the energy cutoff used by Keller and co-workers is high (650 eV). For the van der Waals interaction, the DFT-D3 Grimme method is used and the value taken for the Hubbard U parameter is 4.5 eV. The thickness of the vacuum layer in their surface model is not indicated, but the supercells used are $p(1 \times 2)$, $p(2 \times 2)$, and $p(2 \times 4)$, in our notation. It is not clear, though, which one was used for the adsorptions discussed above.

Given the various dissimilarities between our results and those of the previous works discussed, we report on some of the calculations we performed to verify our findings. A first point is that the initial height at which the CO_2 molecule is set above the surface is typically not stated. Thus, to find out to what extent the height can be the source of a difference, we ran the full calculations for the dh_b and ot_b geometries, as they are representative of our findings, with initial heights of 3.0 and 3.5 Å. We found that the calculations converge to the same adsorption states as before, independently of the initial height. As shown in Table 2, the corresponding adsorption energies are essentially the same. Another aspect of the methodology that could potentially result in clear differences is the approach to the van der Waals interaction. Thus, we considered the three Grimme type of approaches implemented in VASP. We find that although the energetics present noticeable differences, the adsorption states themselves are geometrically basically the same. In the case of dh_b^{α}, the largest difference with our results is ∼0.14 eV, and in the case of ot_b^{α}, it is ∼0.20 eV. Finally, we considered the possible effect of the supercell size. In addition to the $p(2 \times 2)$ supercell, we considered supercells of sizes $p(3 \times 3)$ and $p(4 \times 4)$, as well as five- and seven-layer slabs. In the latter case, the three bottom layers were kept fixed during the relaxation calculations. Since the calculations starting from the initial ot_b geometry lead to the state with strongest interactions, i.e., the ot_b^{α} chemisorbed state, we performed the additional calculations for that case. We note first that the results in Table 2 show that the slab thickness has a negligible effect on the adsorption energy. So with a slab five layers thick, one obtains essentially converged results in this sense. On the other hand, the adsorption energies do show an increase with supercell size. Nevertheless, the increase seems to tend to saturate, as the increase in energy from $p(2 \times 2)$ to $p(3 \times 3)$ is ∼0.11 eV, while the increase from $p(3 \times 3)$ to $p(4 \times 4)$ is ∼0.03 eV. Calculations with larger supercells would be needed to confirm this. This notwithstanding, these results confirm the chemisorbed ot_b^{α} state. We do not expect that calculations on a larger supercell will lead to a qualitatively different result or a significantly different adsorption energy.

5. CONCLUSIONS

In this work, we revisit the question of the adsorption of CO_2 on stoichiometric CeO_2 (110) surfaces using first-principles methods. We identified five distinct adsorption states, one corresponding to chemisorption and four to physisorption. Whether the molecule will be physisorbed or chemisorbed depends highly on both the site approached and the initial molecule orientation relative to the surface. In the chemisorbed state, the CO_2 molecule forms a carbonate species with a surface oxygen. The molecular levels participating more directly in the bonding are the $2\sigma_u$ and, especially, the nonbonding HOMO π_g levels. The surface Ce atoms play a negligible role in the interaction, and the binding is monodentate. Regarding the physisorption states, three of them fall in an energy range corresponding to strong physisorption and one corresponding to moderate physisorption of moderate strength. The mechanism behind the physisorption in all four cases can be considered of the Debye type, i.e., the interaction obeys to the induced dipole moment in the molecule and the polarization of the surface atoms at the site of the adsorption. In the strong physisorption case, the molecule is bent in addition to being polarized more strongly. In the moderate case, the dipole moment induced is linear. In the physisorbed states, the CO_2 molecule conserves its identity. Its molecular levels are disturbed, but their orbital character is preserved. The shifts of the energy levels with respect to the free molecule more clearly reveal the interaction. Finally, our results suggest that chemisorption will occur more often than is physisorption. This is in line with the conclusions of XPS/NEXAFS studies of CO_2 adsorption on oxidized ceria (110), reporting physisorption as a minority species as compared to chemisorption.

■ ASSOCIATED CONTENT

Supporting Information

The Supporting Information is available free of charge at https://pubs.acs.org/doi/10.1021/acs.jpcc.5c01747.

Bulk CeO_2 calculated properties (S1); CeO_2 slab interlayer distances (S2); complementary adsorption data (S3); CeO_2 slab electronic structure (S4); band structure plots for selected adsorption states (S5); Bader charges (S6); and Hirshfeld charges (S7) (PDF)

■ AUTHOR INFORMATION

Corresponding Authors

Rolando Saniz − *CMT, Departement Fysica, Universiteit Antwerpen, Antwerpen B-2020, Belgium; PLASMA Centre of Excellence, Universiteit Antwerpen, Antwerpen B-2610,*

https://doi.org/10.1021/acs.jpcc.5c01747
J. Phys. Chem. C 2025, 129, 12814−12826

Belgium; orcid.org/0000-0001-5764-6791; Email: rolando.saniz@uantwerpen.be

Bart Partoens − *CMT, Departement Fysica, Universiteit Antwerpen, Antwerpen B-2020, Belgium; PLASMA Centre of Excellence, Universiteit Antwerpen, Antwerpen B-2610, Belgium*; Email: bart.partoens@uantwerpen.be

Authors

Shangkun Li − *PLASMANT, Departement Chemie and PLASMA Centre of Excellence, Universiteit Antwerpen, Antwerpen B-2610, Belgium; CMT, Departement Fysica, Universiteit Antwerpen, Antwerpen B-2020, Belgium;* orcid.org/0000-0002-9297-1669

Dirk Lamoen − *EMAT, Departement Fysica, Universiteit Antwerpen, Antwerpen B-2020, Belgium*

Annemie Bogaerts − *PLASMANT, Departement Chemie and PLASMA Centre of Excellence, Universiteit Antwerpen, Antwerpen B-2610, Belgium;* orcid.org/0000-0001-9875-6460

Complete contact information is available at: https://pubs.acs.org/10.1021/acs.jpcc.5c01747

Notes

The authors declare no competing financial interest.

■ ACKNOWLEDGMENTS

Financial support for this project was provided by the Methusalem grant of the University of Antwerp. The computational work was performed in part using HPC resources from the VSC (Flemish Supercomputer Center) and the HPC infrastructure of the University of Antwerp (CalcUA), both funded by the FWO-Vlaanderen and the Flemish Government-Department EWI.

■ REFERENCES

(1) Burghaus, U. Surface chemistry of CO_2 - Adsorption of carbon dioxide on clean surfaces at ultrahigh vacuum. *Prog. Surf. Sci.* **2014**, *89*, 161−217.

(2) Taifan, W.; Boily, J.-F.; Baltrusaitis, J. Surface chemistry of carbon dioxide revisited. *Surf. Sci. Rep.* **2016**, *71*, 595−671.

(3) Tu, X.; Whitehead, J. C.; Nozaki, T., Eds. *Plasma Catalysis: Fundamentals and Applications*; Springer: Cham, Switzerland, 2019.

(4) Bogaerts, A.; Tu, X.; Whitehead, J. C.; Centi, G.; Lefferts, L.; Guaitella, O.; Azzolina-Jury, F.; Kim, H.-H.; Murphy, A. B.; Schneider, W. F.; et al. The 2020 plasma catalysis roadmap. *J. Phys. D: Appl. Phys.* **2020**, *53*, No. 443001.

(5) Loenders, B.; Michiels, R.; Bogaerts, A. Is a catalyst always beneficial in plasma catalysis? Insights from the many physical and chemical interactions. *J. Energy Chem.* **2023**, *85*, 501−533.

(6) Wang, L.; Yi, Y.; Guo, H.; Tu, X. Atmospheric Pressure and Room Temperature Synthesis of Methanol through Plasma-Catalytic Hydrogenation of CO_2. *ACS Catal.* **2018**, *8*, 90−100.

(7) Michiels, R.; Engelmann, Y.; Bogaerts, A. Plasma Catalysis for CO_2 Hydrogenation: Unlocking New Pathways toward CH_3OH. *J. Phys. Chem. C* **2020**, *124*, 25859−25872.

(8) Etim, U. J.; Zhang, C.; Zhong, Z. Impacts of the Catalyst Structures on CO_2 Activation on Catalyst Surfaces. *Nanomaterials* **2021**, *11*, No. 3265.

(9) Ramis, G.; Busca, G.; Lorenzelli, V. Low-temperature CO_2 adsorption on metal oxides: spectroscopic characterization of some weakly adsorbed species. *Mater. Chem. Phys.* **1991**, *29*, 425−435.

(10) Bandi, A.; Schwarz, J.; Maier, C. U. Adsorption of CO_2 on Transition Metals and Metal Oxides. *J. Electrochem. Soc.* **1993**, *140*, 1006−1008.

(11) Seiferth, O.; Wolter, K.; Dillmann, B.; Klivenyi, G.; Freund, H.-J.; Scarano, D.; Zecchina, A. IR investigations of CO_2 adsorption on chromia surfaces: Cr_2O_3 (0001)/Cr(110) versus polycrystalline α-Cr_2O_3. *Surf. Sci.* **1999**, *421*, 176−190.

(12) Mirabella, F.; Zaki, E.; Ivars-Barcelo, F.; Schauermann, S.; Shaikhutdinov, S.; Freund, H.-J. CO_2 Adsorption on Magnetite Fe_3O_4(111). *J. Phys. Chem. C* **2018**, *122*, 27433−27441.

(13) Berland, K.; Cooper, V. R.; Lee, K.; Schröder, E.; Thonhauser, T.; Hyldgaard, P.; Lundqvist, B. I. van der Waals forces in density functional theory: a review of the vdW-DF method. *Rep. Prog. Phys.* **2015**, *78*, No. 066501.

(14) Dai, J.; Yuan, J. Physisorption to chemisorption transition of NO_2 on graphene induced by the interplay of SiO_2 substrate and van der Waals forces: A first principles study. *Chem. Phys.* **2012**, *405*, 161−166.

(15) Huber, F.; Berwanger, J.; Polesya, S.; Mankovsky, S.; Ebert, H.; Giessibl, F. J. Chemical bond formation showing a transition from physisorption to chemisorption. *Science* **2019**, *366*, 235−238.

(16) Ma, L.-J.; Han, T.; Jia, J.; Wu, H.-S. Cooperative physisorption and chemisorption of hydrogen on vanadium-decorated benzene. *RSC Adv.* **2020**, *10*, 37770−37778.

(17) Borodin, D.; Rahinov, I.; Shirhatti, P. R.; Huang, M.; Kandratsenka, A.; Auerbach, D. J.; Zhong, T.; Guo, H.; Schwarzer, D.; Kitsopoulos, T. N.; Wodtke, A. M. Following the microscopic pathway to adsorption through chemisorption and physisorption wells. *Science* **2020**, *369*, 1461−1465.

(18) Benavid, L. I.; Carter, E. A. CO_2 Adsorption on Cu_2O(111): A DFT+U and DFT-D Study. *J. Phys. Chem. C* **2013**, *117*, 26048−26059.

(19) Kumar, A.; Ropital, F.; de Bruin, T.; Diawara, B. Effects of surface orientations of Cr_2O_3 on CO_2 adsorption: A DFT approach. *Appl. Surf. Sci.* **2020**, *529*, No. 147127.

(20) Chávez-Rocha, R.; Mercado-Sánchez, I.; Vargas-Rodriguez, I.; Hernández-Lima, J.; Bazán-Jiménez, A.; Robles, J.; García-Revilla, M. A. Modeling Adsorption of CO_2 in Rutile Metallic Oxide Surfaces: Implications in CO_2 Catalysis. *Molecules* **2023**, *28*, No. 1776.

(21) Trovarelli, A. Catalytic Properties of Ceria and CeO_2-Containing Materials. *Catal. Rev.* **1996**, *38*, 439−520.

(22) Mullins, D. R. The surface chemistry of cerium oxide. *J. Phys. Chem. C* **2015**, *70*, 42−85.

(23) *Catalysis by Ceria and Related Materials*, 2nd ed.; Trovarelli, A.; Fornasiero, P., Eds.; Imperial College Press: London, United Kingdom, 2013.

(24) Montini, T.; Melchionna, M.; Monai, M.; Fornasiero, P. Fundamentals and Catalytic Applications of CeO_2-Based Materials. *Chem. Rev.* **2016**, *116*, 5987−6041.

(25) Boaro, M.; Colussi, S.; Trovarelli, A. Ceria-Based Materials in Hydrogenation and Reforming Reactions for CO_2 Valorization. *Front. Chem.* **2019**, *7*, No. 28.

(26) Mishra, U. K.; Chandel, V. S.; Singh, O. P. A review on cerium oxide-based catalysts for the removal of contaminants. *Emergent Mater.* **2022**, *5*, 1443−1476.

(27) Cheng, Z.; Sherman, B. J.; Lo, C. S. Carbon dioxide activation and dissociation on ceria (110): A density functional theory study. *J. Chem. Phys.* **2013**, *138*, No. 014702.

(28) Kumari, N.; Sinha, N.; Haider, M. A.; Basu, S. CO_2 reduction to methanol on CeO_2 (110) surface: A density functional theory study. *Electrochim. Acta* **2015**, *177*, 21−29.

(29) Lu, X.; Wang, W.; Wei, S.; Guo, C.; Shao, Y.; Zhang, M.; Deng, Z.; Zhu, H.; Guo, W. Initial reduction of CO_2 on perfect and O-defective CeO_2 (111) surfaces: towards CO or COOH? *RSC Adv.* **2015**, *5*, 97528−97535.

(30) Kumari, N.; Haider, M. A.; Agarwal, M.; Sinha, N.; Basu, S. Role of Reduced CeO_2(110) Surface for CO_2 Reduction to CO and Methanol. *J. Phys. Chem. C* **2016**, *120*, 16626−16635.

(31) Cheng, Z.; Lo, C. S. Mechanistic and microkinetic analysis of CO_2 hydrogenation on ceria. *Phys. Chem. Chem. Phys.* **2016**, *18*, 7987−7996.

(32) Cao, F.; Xiao, Y.; Zhang, Z.; Li, J.; Xia, Z.; Hu, X.; Ma, Y.; Qu, Y. Influence of oxygen vacancies of CeO_2 on reverse water gas shift reaction. *J. Catal.* **2022**, *414*, 25−32.
(33) Tumuluri, U.; Rother, G.; Wu, Z. Fundamental Understanding of the Interaction of Acid Gases with CeO_2: From Surface Science to Practical Catalysis. *Ind. Eng. Chem. Res.* **2016**, *55*, 3909−3919.
(34) Symington, A. R.; Harker, R. M.; Storr, M. T.; Molinari, M.; Parker, S. C. Thermodynamic Evolution of Cerium Oxide Nanoparticle Morphology Using Carbon Dioxide. *J. Phys. Chem. C* **2020**, *124*, 23210−23220.
(35) Zhu, D.; Liu, H.; Huang, Y.; Luo, X.; Mao, Y.; Liang, Z. Study of Direct Synthesis of DMC from CO_2 and Methanol on CeO_2: Theoretical Calculation and Experiment. *Ind. Eng. Chem. Res.* **2022**, *61*, 10804−10817.
(36) Gao, J.; Yang, J.-W.; Ma, T.; Wang, J.; Xia, D.; Du, B.; Cui, Y.; Yang, C. Mechanism study on direct synthesis of glycerol carbonate from CO_2 and glycerol over shaped CeO_2 model catalysts. Chinese. *Chem. Lett.* **2023**, *34*, No. 108395.
(37) Keller, F.; Dön, J.; Groß, A.; Busch, M. Exploring the Mechanism of the Electrochemical Polymerization of CO_2 to Hard Carbon over CeO2(110). *J. Phys. Chem. C* **2024**, *128*, 6280−6293.
(38) Buckingham, A. D.; Disch, R. L.; Dunmur, D. A. The Quadrupole Moments of Some Simple Molecules. *J. Am. Chem. Soc.* **1968**, *90*, 3104−3107.
(39) Margenau, H. The role of quadrupole forces in van der Waals attractions. *Phys. Rev.* **1931**, *38*, 747−756.
(40) London, F. The general theory of molecular forces. *Trans. Faraday Soc.* **1937**, *33*, 8b−26.
(41) Jiang, X. P.; Toigo, F.; Cole, M. W. Quadrupole contribution to the physisorption interaction. *Chem. Phys. Lett.* **1983**, *101*, 159−162.
(42) Yang, C.; Bebensee, F.; Chen, J.; Yu, X.; Nefedov, A.; Wöll, C. Carbon Dioxide Adsorption on CeO_2(110): An XPS and NEXAFS Study. *ChemPhysChem* **2017**, *18*, 1874−1880.
(43) Kresse, G.; Hafner, J. Ab initio molecular dynamics for liquid metals. *Phys. Rev. B* **1993**, *47*, 558−561.
(44) Kresse, G.; Furthmüller, J. Efficiency of ab-initio total energy calculations for metals and semiconductors using a plane-wave basis set. *Comput. Mater. Sci.* **1996**, *6*, 15−50.
(45) Kresse, G.; Furthmüller, J. Efficient iterative schemes for ab initio total-energy calculations using a plane-wave basis set. *Phys. Rev. B* **1996**, *54*, 11169−11186.
(46) Blöchl, P. E. Projector augmented-wave method. *Phys. Rev. B* **1994**, *50*, 17953−17979.
(47) Kresse, G.; Joubert, D. From ultrasoft pseudopotentials to the projector augmented-wave method. *Phys. Rev. B* **1999**, *59*, 1758−1775.
(48) Perdew, J. P.; Burke, K.; Ernzerhof, M. Generalized Gradient Approximation Made Simple. *Phys. Rev. Lett.* **1996**, *77*, 3865−3868.
(49) Dudarev, S. L.; Botton, G. A.; Savrasov, S. Y.; Humphreys, C. J.; Sutton, A. P. Electron-energy-loss spectra and the structural stability of nickel oxide: An LSDA+U study. *Phys. Rev. B* **1998**, *57*, 1505−1509.
(50) Dion, M.; Rydberg, H.; Schröder, E.; Langreth, D. C.; Lundqvist, B. I. Van der Waals Density Functional for General Geometries. *Phys. Rev. Lett.* **2004**, *92*, No. 246401.
(51) Román-Pérez, G.; Soler, J. M. Efficient Implementation of a van der Waals Density Functional: Application to Double-Wall Carbon Nanotubes. *Phys. Rev. Lett.* **2009**, *103*, No. 096102.
(52) Klimeš, J.; Bowler, D. R.; Michaelides, A. Van der Waals functionals applied to solids. *Phys. Rev. B* **2011**, *83*, No. 195131.
(53) Nolan, M.; Grigoleit, S.; Sayle, D. C.; Parker, S. C.; Watson, G. W. Density functional theory studies of the structure and electronic structure of pure and defective low index surfaces of ceria. *Surf. Sci.* **2005**, *576*, 217−229.
(54) In the Dudarev approach, only the difference between the on-site Coulomb and exchange parameters enters the Hubbard term. So implicitly $J = 0$ is taken for the exchange parameter.
(55) Birch, F. Finite elastic strain of cubic crystals. *Phys. Rev.* **1947**, *71*, 809−824.
(56) Gerward, L.; Olsen, J. S. Powder diffraction analysis of cerium dioxide at high pressure. *Phys. Rev.* **1993**, *8*, 127−129.
(57) Note that it is well-known that GGA-based calculations typically slightly overestimate lattice parameters
(58) Blöchl, P.; Jepsen, O.; Andersen, O. K. Improved tetrahedron method for Brillouin-zone integrations. *Phys. Rev. B* **1994**, *49*, 16223−16233.
(59) Tkatchenko, A.; Scheffler, M. Accurate Molecular Van Der Waals Interactions from Ground-State Electron Density and Free-Atom Reference Data. *Phys. Rev. Lett.* **2009**, *102*, No. 073005.
(60) Bultinck, P.; Alsenoy, C. V.; Ayers, P. W.; Carbó-Dorca, R. Critical analysis and extension of the Hirshfeld atoms in molecules. *J. Chem. Phys.* **2007**, *126*, No. 144111.
(61) Damme, S. V.; Bultinck, P.; Fias, S. Electrostatic potentials from self-consistent Hirshfeld atomic charges. *J. Chem. Theory Comput.* **2009**, *5*, 334−340.
(62) Bučko, T.; Lebègue, S.; Ángyán, J. G.; Hafner, J. Extending the applicability of the Tkatchenko-Scheffler dispersion correction via iterative Hirshfeld partitioning. *J. Chem. Phys.* **2014**, *141*, No. 034114.
(63) For this we use the code developed by Henkelman's group at the University of Texas at Austin. Please see:. https://theory.cm.utexas.edu/henkelman/code/bader/.
(64) Momma, K.; Izumi, F. VESTA 3 for three-dimensional visualization of crystal, volumetric and morphology data. *J. Appl. Crystallogr.* **2011**, *44*, 1272−1276.
(65) MATLAB version: 24.2.0.2712019 (R2024b), Natick, Massachusetts: The Mathworks Inc.; 2024.
(66) Arts, I.; Saniz, R.; Baldinozzi, G.; Leinders, G.; Verwerft, M.; Lamoen, D. Ab initio study of the adsorption of O, O_2, H_2O and H_2O_2 on UO_2 surfaces using DFT+U and non-collinear magnetism. *J. Nucl. Mater.* **2024**, *599*, No. 155249.
(67) This is the slight split of the Ce-O layers discussed previously
(68) Allan, C. J.; Gelius, U.; Allison, D.; Johansson, G.; Siegbahn, H.; Siegbahn, K. ESCA studies of CO_2, CS_2, and COS. *J. Electron Spectrosc. Relat. Phenom.* **1972**, *1*, 131−151.
(69) We were unable to find a more recent experimental report on the energy spectrum of the CO_2 molecule.
(70) Atkins, P.; de Paula, J.; Keeler, J. *Physical Chemistry*, 11th ed.; Oxford University Press: Oxford, United Kingdom, 2018.
(71) Choi, W. S.; Lee, H. N. Strain tuning of electronic structure in $Bi_4Ti_3O_{12}$-$LaCoO_3$ epitaxial thin films. *Phys. Rev. B* **2015**, *91*, No. 174101.
(72) The energy value of the lowest Ce 5*s*was chosen so that the valence band maximum is at 0.
(73) Among the unoccupied levels, the $5\sigma_g$ and $4\sigma_u$ are not discernible, as they are largely hybridized with surface levels. This is of no consequence for the analysis below.
(74) Mind that small values like 0.004*e* might fall within the error margin.
(75) See Supporting Information for more on the Hirshfeld-I charges
(76) In the previous Section we mentioned that the surface Ce-O top layer is jagged (see Figure 1), which probably confers the surface some mild dipole moment. This might have an effect on the mechanism described, but whether it is of any significance is difficult to assess. The same comment applies to the adsorption cases discussed in the following.
(77) Yanagisawa, S.; Hamada, I.; Lee, K.; Langreth, D. C.; Morikawa, Y. Adsorption of Alq_3 on Mg(001) surface: Role of chemical bonding, molecular distortion, and van derWaals interaction. *Phys. Rev. B* **2011**, *83*, No. 235412.
(78) Vlaisavljevich, B.; Huck, J. M.; Hulvey, Z.; Lee, K.; Mason, J. A.; Neaton, J. B.; Long, J. R.; Craig M Brown, D. A.; Michaelides, A.; et al. Performance of Van der Waals Corrected Functionals for Guest Adsorption in the M_2(dobdc) Metal-Organic Frameworks. *J. Phys. Chem. A* **2017**, *121*, 4139−4151.
(79) Freire, R. L. H.; Guedes-Sobrinho, D.; Kiejna, A.; Silva, J. L. F. D. Comparison of the Performance of van der Waals Dispersion

Functionals in the Description of Water and Ethanol on Transition Metal Surfaces. *J. Phys. Chem. C* **2018**, *122*, 1577−1588.
(80) It appears that they used a nonlocal functional for this, but no details are given
(81) Hahn, K. R.; Iannuzzi, M.; Seitsonen, A. P.; Hutter, J. Coverage Effect of the CO_2 Adsorption Mechanisms on CeO_2 (111) by First Principles Analysis. *J. Phys. chem. C* **2013**, *117*, 1701−1711.

https://doi.org/10.1021/acs.jpcc.5c01747
J. Phys. Chem. C 2025, 129, 12814−12826